Quantum Information and Computation, Vol. 2, No. 4 (2002) 257–271

TRANSPORT OF QUANTUM STATES AND SEPARATION OF IONS IN A DUAL RF ION TRAP*

M. A. ROWE[†], A. BEN-KISH[‡], B. DEMARCO, D. LEIBFRIED, V. MEYER, J. BEALL[§], J. BRITTON, J. HUGHES, W. M. ITANO, B. JELENKOVIĆ, C. LANGER, T. ROSENBAND, and D. J. WINELAND

Time and Frequency Division, National Institute of Standards and Technology, 325 S. Broadway, Boulder, Colorado 80305-3328

Received April 4, 2002
Revised April 24, 2002

We have investigated ion dynamics associated with a dual linear ion trap where ions can be stored in and moved between two distinct locations. Such a trap is a building block for a system to engineer arbitrary quantum states of ion ensembles. Specifically, this trap is the unit cell in a strategy for scalable quantum computing using a series of interconnected ion traps. We have transferred an ion between trap locations 1.2 mm apart in 50 μs with near unit efficiency ($> 10^6$ consecutive transfers) and negligible motional heating, while maintaining internal-state coherence. In addition, we have separated two ions held in a common trap into two distinct traps.

Keywords: atom trapping and cooling, laser cooling, quantum computation, quantum state engineering, trapped ions
Communicated by: B Kane & R Blatt

1. Introduction

Developing a practical method for synthesizing and manipulating entangled quantum states of many particles is challenging. One approach is to physically isolate small subsystems that can be operated on independently. By entangling these subsystems sequentially or in parallel a large entangled state can be constructed [1]. Some of the elements required for this approach, in the context of trapped ions, are demonstrated here.

For quantum information processing, it may be desirable to transport quantum states between nodes of a larger system for various technical or intrinsic reasons (e.g., in communication systems). In a quantum computer, the carriers might be photons [2] - [4], electron spins [5] - [7], atomic ions [8, 9], or neutral atoms that are transported with guides [10] - [17] or movable potentials [18] - [20]. For ions, this basic idea has also been applied to atomic clocks [21] and cavity-QED studies [22].

*Contribution of the National Institute of Standards and Technology; not subject to U.S. copyright.
[†]present address: Optoelectronics Division, NIST Boulder.
[‡]present address: Technion, Haifa, Israel
[§]Electromagnetic Technology Division, NIST Boulder

There are stringent requirements for a quantum computing system where perhaps hundreds or thousands of two-level quantum systems (qubits) interact. Cirac and Zoller [23] proposed a physical scheme to implement quantum computing using a string of ions that are held in a single linear RF trap. Two internal states of each ion form a qubit. An applied focused laser field selectively couples the qubits to a shared quantized vibrational mode of the trap. Gate operations between qubits are implemented by way of this common vibrational mode that acts as a data bus.

The Cirac-Zoller scheme provides a good starting point for quantum operations, but as the number of ions increases several difficulties are encountered. The addition of each ion to the string adds three vibrational modes. It soon becomes nearly impossible to spectrally isolate the desired vibrational mode unless the speed of operations is slowed to undesirable levels [8, 24]. In addition, as ions are added to the trap the axial trap strength must be decreased in order to maintain a linear string of ions [25]. A weaker trap makes sideband laser cooling less efficient and aggravates the problem of mode isolation due to multimode excitations [8]. Furthermore, since error correction will most likely be incorporated into any large processor, it will be desirable to measure and reset ancilla qubits without disturbing the coherence of logical qubits. Since ion qubits are typically read out using laser scattering, the scattered light from ancilla qubits held in a common trap may disturb the coherence of the logical qubits.

For these reasons, we have considered an architecture that employs an array of interconnected ion traps [8, 26]. Ions are moved between nodes in the array by applying time-dependent potentials to "control" electrode segments. To perform logic operations between selected ions, these ions are transferred into an "accumulator" trap for the gate operation. Before the gate operation is performed, it may be necessary to sympathetically re-cool the qubit ions with another ion species [8]. Subsequently, these ions are moved to memory locations or other accumulators. This strategy always maintains a relatively small number of motional modes that must be considered and minimizes the problems of ion/laser-beam addressing using focused laser beams. Such arrays also enable highly parallel processing and ancilla qubit readout in a separate trapping region so that the logical ions are shielded from the scattered laser light. In the work reported here, we have implemented the first steps towards realizing this architecture. By continually changing the electric potentials on a series of electrode segments, we were able to smoothly translate our trapping potential and move ions adiabatically between two locations in a simple "dual-trap" array. In addition, by increasing the potential on an electrode near two ions, a potential wedge was inserted between the ions, separating them into the two traps.

2. The Trap

The trap was constructed from a stack of metallized 200 μm thick alumina wafers. Laser-machined slots and gold traces created the desired electrode geometry as in the traps of Ref. [27]. Gold traces of 0.5 μm thickness were made with evaporated gold that was transmitted through a shadow mask and deposited on the alumina. Subsequently, an additional 3 μm of gold was electroplated onto the electrodes, resulting in electrode surfaces smooth at the 1 μm level. These lithographic techniques allow for small traps and could be expandable to larger arrays. The idealized four-rod linear trap geometry (Fig. 1a) is approximated using a wafer stack (Figs. 1b and 1c). The central slot width (400 μm) and the wafer spacing (360 μm) set

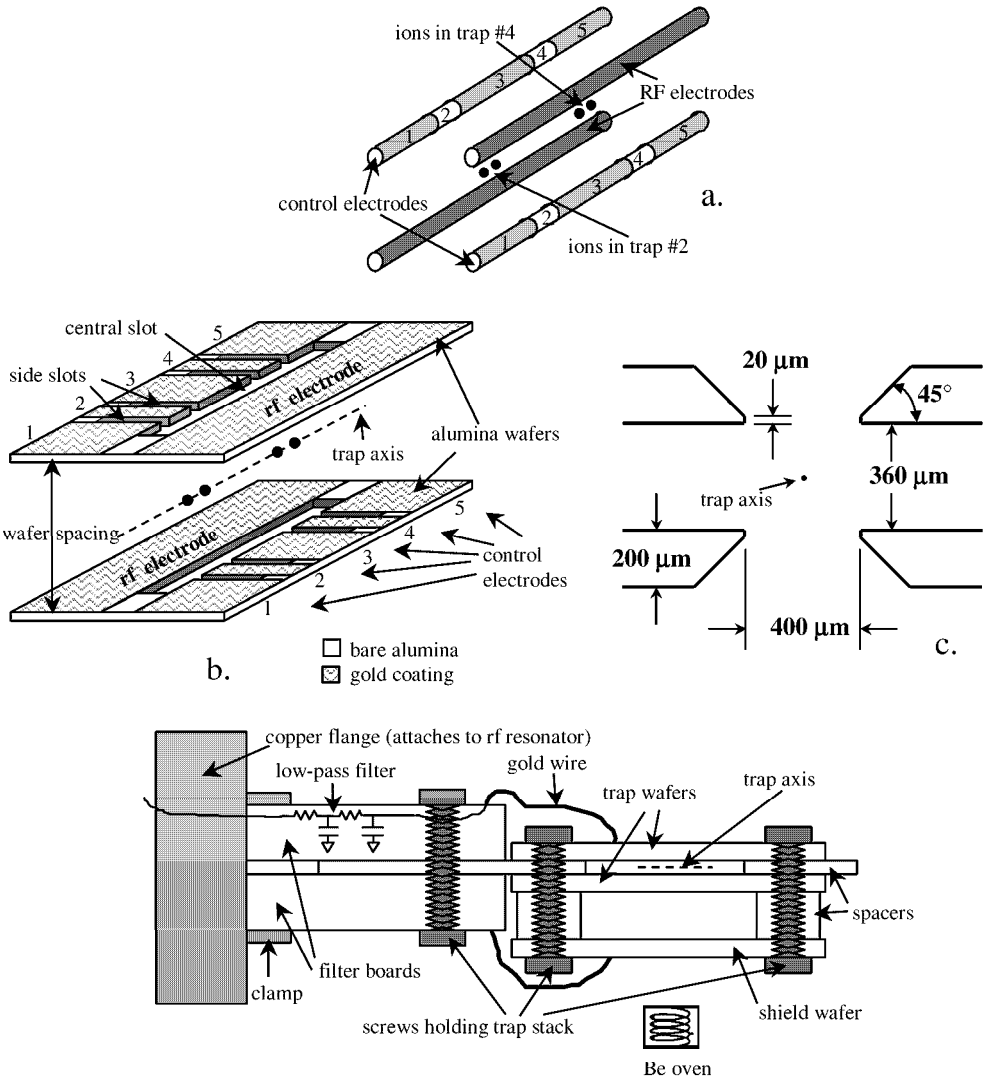

Fig. 1. The dual linear ion trap (drawings not to scale). a. The idealized four-rod geometry. b. The wafer-stack implementation. The two trap wafers are spaced with two 360 μm thick alumina pieces (not shown) that are placed between them along the short edges. The pairs of control electrodes are numbered 1 through 5 for reference. The two trap locations, #2 and #4, shown in the figure are labeled by the electrode on which they are centered. The axial length of electrode 1 (2,3,4,5) is 1100 μm (400 μm, 800 μm, 400 μm, 1100 μm). For 8.0 V applied to electrodes 1, 3, and 5 and 0.0 V applied to electrodes 2 and 4 the axial trap frequency in each trap was 2.9 MHz for a single $^9Be^+$ ion. The peak amplitude of the applied RF voltage was about 500 V. The RF drive frequency was 230 MHz. c. Cross-section of the trap electrodes (looking along the trap axis). d. Side view assembly diagram of the trap structure.

the length scale of the RF trap. The side slots (10 μm wide) electrically isolate the different control electrodes.

The control electrodes (held at RF ground) are arranged into five segments for axial confinement (Fig. 1b). Radial confinement (perpendicular to the axial direction) is provided primarily by ponderomotive forces generated by potentials applied to the RF electrodes [8]. Ions can be trapped at various locations along the axis. For instance, confinement (of positive ions) at two distinct places occurs when the outer two and middle segments are biased above the remaining two segments as shown schematically in Fig. 1a.

A new feature of this trap compared to our previous ones is the line-of-sight shielding of the electrodes from the neutral beryllium oven source (located about 2 cm from the trap). Previous evidence [27] indicated that the heating rate of an ion's motional state increased over time as beryllium was deposited onto the electrodes. In all of our experiments, the source of beryllium has been a tungsten/beryllium filament that was heated with direct current thereby emitting beryllium atoms towards the trap electrodes. Some of the beryllium atoms that pass through the trap are ionized by electrons that are also directed through the trap; the resulting $^9Be^+$ ions are then confined. During trap loading the beryllium is emitted in all directions and in previous designs was able to coat the electrodes. In the current trap, the electrodes were shielded from this beryllium flux by a shadow mask. This consisted of an alumina wafer with a single 200 μm wide slot cut along its center line that was positioned 700 μm above the trap wafer nearest to the oven. This shield wafer prevented deposition of beryllium on any part of the trap electrodes. Gold was deposited onto a rectangular area centered around the slot in the shield and facing the trap electrodes. Voltage applied to the shield's gold trace in combination with a differential voltage applied between diagonal pairs of the control electrodes (for example, between the #2 electrodes in trap #2) allowed us to compensate for micromotion in at least one of the traps [28].

Figure 1d shows a schematic of the entire trap structure. The two trap wafers and the shield wafer were spaced with 360 μm thick alumina wafers along the short edges. The central and side slots were unobstructed by these spacers. The entire stack of wafers was held together with two 000-120 screws (one on each end of the wafer stack) passing through the trap axis. Two "filter boards" held the wafer stack via a mutual spacer board and an additional screw. A cascade of two RC low-pass filters (R= 1 kΩ, C= 820 pF) was connected to each control electrode by a gold wire. The trap stack was clamped inside a resonator that applied up to about 500 V at 230 MHz to the RF electrodes [29], which were electrically common. This trap assembly was encased in a quartz envelope attached to a stainless steel vacuum chamber. After cleaning, the system was baked at 300° C for about two days, resulting in a final ambient pressure that was less than 4×10^{-9} Pa (3×10^{-11} Torr).

3. The Apparatus

We confine $^9Be^+$ ion qubits in this trap. We spectrally resolve two of the ions' ground-state hyperfine levels, $F = 2, m_F = -2$ and $F = 1, m_F = -1$ whose wave functions are labeled $|\downarrow\rangle$ and $|\uparrow\rangle$ respectively. The frequency splitting between these two levels, $\omega_0/2\pi$, is approximately 1.25 GHz. We must also account for the quantized motional levels due to the ions' confinement by the trap potential. For a given motional mode, these realize a ladder of states labeled $|n\rangle$ where $n = 0, 1, 2, \rightarrow \infty$. We cool to the ground state ($n = 0$) with Doppler cooling followed

Table 1. Summary of ambient heating results for three different traps. The heating rates are expressed as 1 quantum absorbed per unit of time and ν_z is the trap axial frequency.

Trap	heating rate ($\nu_z = 2.9$ MHz)	heating rate ($\nu_z = 3.9$ MHz)	edge plating	electro-plated	electrode shield	electrode distance (d)
dual	1/10 ms (initial) 1/4 ms (later)	1/8 ms	yes	yes	yes	270 μm
trap A	$\approx$ 1/100 μs	$\approx$ 1/100 μs	no	no	no	220 μm
trap C	—	1/4 ms (initial) 1/1 ms (later)	yes	no	no	220 μm

by Raman sideband cooling [30, 31]. "Repump" lasers optically pump an ion to $|\downarrow\rangle$, thereby initializing the internal state [30]. We drive stimulated-Raman transitions with laser beams to coherently move population between the atomic and motional levels [32, 33]. The two Raman beams have a wavelength $\lambda \simeq 313$ nm and a difference frequency near $\omega_0/2\pi$. They are aligned either parallel (0° geometry) or perpendicular (90° geometry) to each other, with their difference wave vectors, $\vec{\Delta k} \simeq 0$ or $|\vec{\Delta k}| \simeq \frac{2\sqrt{2}\pi}{\lambda}$ along the trap axis respectively. The final state is determined by probing the ion with circularly polarized light from a "detection" laser. During the 200 μs detection period, ions in the $|\downarrow\rangle$ state scatter many photons, while ions in the $|\uparrow\rangle$ state scatter few photons. The total number of fluorescence photons collected during the detection period indicate the final spin state [33, 34].

4. Ambient Ion Heating

The ambient heating of the motional modes is an important source of decoherence for the Cirac/Zoller gates, which proceed through specific vibrational levels [23]. An expected source of heating is that caused by thermal electronic noise [8]. However, the heating that we have observed has always been significantly above what is expected from this source and may be due to fluctuating patch potentials on the electrode surfaces [27]. Compared to our previous results [27], the results for the dual trap given below show that the ambient heating has been significantly reduced.[¶] Our heating figure of merit, the time interval to absorb one motional quantum from the ground state ($\approx$ 10 ms) divided by the entangling gate period ($\approx$ 10 μs), approaches 1000. The information below compares the results from three different traps and is summarized in Table 1.

We determined the ambient motional heating rate for the axial mode (frequency ν_z) of a single ion in the trap. The ion's axial motion is first cooled to the ground state. Following this, the thermal motional state, quantified by the mean populated motional level $\langle n_z \rangle$, was measured for various delay times by use of a standard sideband comparison technique [27, 30]. The heating rate, $\partial\langle n_z \rangle/\partial t$, was initially measured to be 1 quantum/10 ms for $\nu_z = 2.9$ MHz. This rate is about 100 times smaller than in a previous trap[‖] (referred to here as trap A), which was made with similar construction (evaporated gold on alumina wafers but no electroplating). The characteristic distance d, which we take as the distance from the ion to the nearest trap

[¶] Heating results from several trapped ion experiments are summarized in Refs. [27] and [35]. Here we limit our comparison to $^9Be^+$ heating in traps with very similar construction.

[‖] Trap 6 in Ref. [27].

electrode, is about 25 % larger for the dual trap than trap A.** The approximate d^{-4} scaling of the heating rate found in Ref. [27] predicts that the heating rate in the dual trap should be smaller by only about a factor of 2 than in trap A. The heating rate in the dual trap increased to approximately 1 quantum/4 ms after a period of about 2 weeks, but the rate stabilized to this value for the next 6 months or about 1000 trap loads.

The line-of-sight shielding of the electrodes from beryllium deposition appears to explain some of the improvement. However, measurements of heating rates for another recently-constructed trap (referred to here as trap C) indicate that beryllium contamination may not be the only source of heating. Trap C was a duplicate of trap A (about the same dimensions and no electrode shielding) except that additional care was taken with the electrode surfaces. For both trap C and the dual trap we made sure that the evaporated gold layer was even and continuous over the edges of all of the electrodes nearest to the ions. The initial heating rate in trap C (when the beryllium deposition was minimal) was 1 quantum per 4 ms for $\nu_z =$ 3.9 MHz. This rate is also much smaller (about a factor of 35) than the rate in trap A with $\nu_z = 3.9$ MHz. However, after about 100 loads (the extent of our data) the heating rate in trap C increased to about 1 quantum per 1 ms. The heating rate in the dual trap with $\nu_z =$ 3.9 MHz was 1 quanta per 8 ms (after 2 weeks of operation). The lower heating rate of the dual trap relative to the initial heating rate in trap C could be explained by the electroplating of the dual trap's electrodes (the electrodes of traps A and C were not electroplated), some initial beryllium contamination on trap C (before the first heating measurements were carried out), the size scaling ($\approx d^{-4}$), or some combination of these factors. Nevertheless, from these results, electrode surface purity and smoothness appear to be closely correlated with ion heating.

We can estimate the heating from thermal electronic noise in the following way [8]: Since the wavelengths of radiation corresponding to the frequencies of ion motion are much larger than the trap structures, electric fields from blackbody radiation (thermal electronic noise) are strongly altered from their free-space values. The fluctuating fields can be determined by estimating the Johnson noise potential on each electrode from electrode resistance and from resistors purposely attached to the electrodes. Here, we expect this resistance to be dominated by that from the RC filters attached to each control electrode. To estimate the field at the position of the ion, we have numerically solved for the potentials inside the trap structure. For example, for a 1 V potential applied to one of the #1 electrodes we find the axial field at the center of trap #2 to be 2.42 V/cm. Using this value and assuming the RC-filter resistors are at the ambient temperature ($\sim$ 300 K), we estimate the axial heating to be approximately 4 quanta per second for $\nu_z = 2.9$ MHz. Therefore the heating appears to be dominated by causes other than thermal electronic noise [27].

5. Ion Transfer

We transferred an ion from trap #2 to trap #4 (Fig. 1) and back by continuously changing the potentials on the five pairs of control electrodes. This translated the position z_0 of the axial trap minimum between the two trap locations. We initially prepared the ion in the $|\downarrow\rangle|n_z = 0\rangle$ state, where here we consider only the axial mode. Using numerical solutions for

** Some of the sizes, d, listed in Table I of Ref. [27] are incorrect. The size for traps 4 and 5 should be 160 μm. The size for trap 6 (referred to here as trap A) should be 220 μm.

Table 2. The number of axial quanta gained, Δn_z, as a result of transferring the ion from trap #2 to trap #4 and back with a one-way transfer time interval T. The axial trap frequency, ν_z = 2.9 MHz.

T (μs)	Δn_z
16	nonadiabatic
28	0.6±0.2
43	0.04±0.03
54	0.01±0.03
200	0.07±0.06
300	0.00±0.07
590	0.1±0.1

our trap geometry, trap potentials were designed so that during the translation, ν_x, ν_y, and ν_z would be held constant; for the experiments reported here, $\nu_z = 2.9$ MHz. Starting at time $t = 0$ in trap #2 ($z_0 = 0$) the axial trap position was smoothly translated according to

$$z_0(t) = sin^2\left(\frac{\pi t}{2T}\right) \cdot 1.2\,\text{mm} \tag{1}$$

until time $t = T$, after which the axial trap remained at 1.2 mm, the position of trap #4. After a hold period approximately equal to T in trap #4 the transfer process was reversed. Following the transfer back to trap #2 we measured the $\langle n_z \rangle$ as described above.

To determine the motional heating due to the transfer we also measured the motional state of the ion held in trap #2 after the same total time delay. Table 2 gives the results for the ion's motional heating due to transfer back and forth (the heating in the non-transfer case subtracted from the heating in the dynamic case). For $T = 16$ μs, the measured motional sidebands were the same size. This implies that very little population remained in the motional ground state after transfer [27, 30] and that the transfer was no longer adiabatic. For $T = 28$ μs about half a quantum on average was gained due to transfer. From a numerical integration of the classical equations of motion we expected that the ion should gain the amount of energy equal to one motional quantum for a 30 μs transfer duration. This estimate indicates approximately when the transfers are no longer adiabatic and agrees reasonably well with our observations. Overall, this transfer process is robust in that we have not observed any ion loss due to transfer. As an example, in a series of experiments for $T = 54$ μs we transferred the same ion over 10^6 times. In addition, we measured the heating of the two radial motional modes (frequencies between 4 and 5 MHz) due to transfer. For $T = 54$ μs the heating for both of these modes was less than 1 quantum.

6. Coherence Test

A critical requirement for the viability of the multiplexed system envisioned here is that the internal coherence of the ions is maintained as they are moved. We verified this with a Ramsey-type interference experiment. After laser cooling to the $|\downarrow\rangle|n_z = 0\rangle$ state in trap #2, we carried out the transformation

$$|\downarrow\rangle \rightarrow \frac{1}{\sqrt{2}}\left(|\downarrow\rangle + |\uparrow\rangle\right) \tag{2}$$

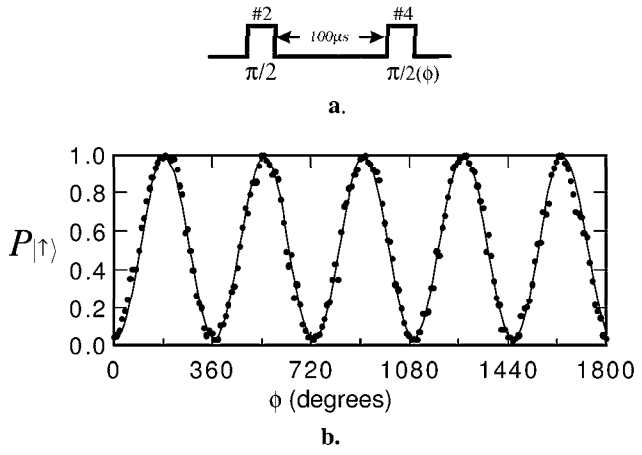

Fig. 2. Coherence transfer experiment. a. The experimental timing. b. The probability for the final state to be $|\uparrow\rangle$, $P_{|\uparrow\rangle}$, as a function of the phase, ϕ, of the final $\pi/2$ pulse. Each graphed point is the result of 200 individual experiments. The probability, $P_{|\uparrow\rangle}$, is the fraction of these experiments with 3 or fewer photons detected during the detection period. (When the ion was in the $|\downarrow\rangle$ state, the mean number of detected photons was 12.)

by applying a $\pi/2$ pulse using the 0° geometry for the Raman laser beams. We then transferred the ion from trap #2 to trap #4 in $T \simeq 55$ μs. The coherence of the internal state remaining after transfer was measured with a final Raman $\pi/2$ pulse (0° geometry) in trap #4 with a controllable phase ϕ relative to the first pulse [8], which was varied. The ion was then moved back to trap #2 for state measurement. The probability $P_{|\uparrow\rangle}$ of finding the final state of the ion to be $|\uparrow\rangle$ is

$$P_{|\uparrow\rangle} = \frac{1}{2}\left(1 + C\cos(\phi + \phi')\right) \tag{3}$$

where ϕ' is a constant laser phase difference between traps #2 and #4. The fringe contrast C is a measure of the coherence [36]. Figure 2a shows the timing of the overall experiment. The length of the $\pi/2$ pulses was 1 to 2 μs. The interval between $\pi/2$ pulses was 100 μs. Figure 2b shows the oscillation in $P_{|\uparrow\rangle}$ as ϕ was varied. The fringe contrast was 95.8 ± 0.8 %, indicating the preservation of coherence. This experiment was line-triggered (60 Hz) to minimize the loss of contrast due to magnetic fields fluctuating at 60 Hz and harmonics of 60 Hz. The data for Figure 2b were taken with 37,000 consecutive round-trip transfers of the same ion.

In another experiment we used a spin-echo technique to minimize the effect of fluctuating magnetic fields so we could trigger the experiment without 60 Hz synchronization. The qubit transition frequency depends on magnetic field ($\simeq 2.1 \times 10^{10}$ Hz-T^{-1}), so the internal state of the ion accumulates an uncontrolled phase between $|\uparrow\rangle$ and $|\downarrow\rangle$ during the free-evolution period between $\pi/2$ pulses due to a time-varying ambient magnetic field. This uncontrolled phase causes the Ramsey fringes to partially wash out after averaging over many experiments, but since the magnetic field changes negligibly during the time of a single experiment we are able to correct for it. By inserting a π pulse between the two Ramsey pulses the phase accumulated during the first half of the Ramsey period is cancelled by that accumulated during the second

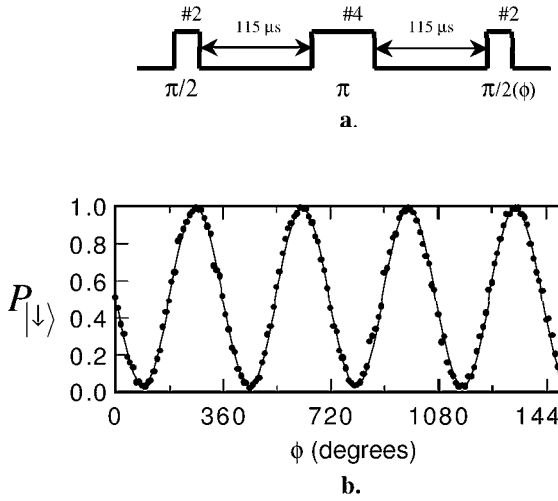

Fig. 3. Spin-echo coherence transfer experiment. a. The experimental timing. b. The probability for the final state to be $|\uparrow\rangle$, $P_{|\uparrow\rangle}$, as a function of the phase, ϕ, of the final $\pi/2$ pulse. Each graphed point is the result of 1000 individual experiments. The probability, $P_{|\uparrow\rangle}$, is the fraction of these experiments with 3 or fewer photons detected during the detection period. (When the ion was in the $|\downarrow\rangle$ state, the mean number of detected photons was 12.) The two $\pi/2$ pulses were generated from separate sources which had a constant phase offset; therefore, a minimum does not occur for $\phi = 0$ as would otherwise be expected.

half.

Figure 3a shows the timing for this experiment. Here, we applied both $\pi/2$ pulses in trap #2. Between these $\pi/2$ pulses we transferred the ion to trap #4 where we applied the π pulse. Figure 3b shows the oscillation in $P_{|\uparrow\rangle}$ as the phase of the final $\pi/2$ pulse, ϕ, was scanned. The fringe contrast is 96.6 ± 0.5 %. These data were taken with 170,000 consecutive round-trip transfers of the same ion. In a control experiment we applied the same pulses and timing but did not transfer the ion (the π pulse was applied in trap #2). For these data we measured a fringe contrast equal to 96.8 ± 0.3 %. The reduction in fringe contrast from 100 % in the control experiment is due to factors other than transfer decoherence, such as imperfect Raman pulses and imperfect state preparation and detection. The decrease in fringe contrast due to transferring the ion both ways was 0.2 ± 0.6 %. Therefore, within experimental error, we see no reduction in the internal state coherence of the ion due to transfer.

7. Separating Ions

As a test of separating ions, we confined two ions in trap #2, separated them into traps #2 and #4 (1.2 mm apart), and then brought them back together in trap #2. The separation sequence began with laser cooling in trap #2 after which the two ions were transferred from trap #2 to trap #3. Prior to separation, the axial center-of-mass frequency in trap #3 was adjusted to 700 kHz (8V, 0V, 0V, 0V, 8V on electrodes 1 through 5 respectively). Following this, the potential on electrodes 3 was raised. Initially this process weakened the axial confinement common to both ions. The trap potentials were smoothly varied so that after approximately

2 ms, the lowest center-of-mass axial frequency (90 kHz) was reached, at which point two separate potential wells developed with one ion in each well.[††] From this point, the individual ion axial frequencies were smoothly increased to about 2.9 MHz. During the separation, the x and y mode frequencies smoothly varied and were bounded between 3 and 7 MHz. We found that by raising the potentials on electrodes 1 and 5 in addition to electrodes 3 during separation, we had finer control over the ion motion. The potential barriers from electrodes 1 and 5 prevented the ions from "rolling down" the potential hill created by electrodes 3, making the process less sensitive to voltage fluctuations on electrodes 3. Even with this strategy we had to raise the potential on electrodes 3 in a precisely controlled manner. For example, the finite voltage steps ($\approx$ 10 mV) in the output of the digital waveform generators applied to the electrodes heated the ions. We filtered these potential steps with an additional cascade of two RC low-pass filters (R = 1 kΩ, C = 22 nF) inserted before the control electrode filters shown in Fig. 1d. When the ions were finally separated into traps #2 and #4, the voltages on the electrodes were respectively 8V, 0V, 8V, 0V, 8V on electrodes 1 through 5. The axial frequency ν_z was equal to 2.9 MHz in each of these traps. In the separation process, the trajectories of the ions were designed to start and end with zero velocity and acceleration; the acceleration between these end points was a (smooth) polynomial function. In the experiments reported here, we used a total period of $\approx$ 10 ms to separate the ions from trap #3 to traps # 2 and 4. This process was reversed to bring the ions back together in trap #2.

In order to demonstrate separation of the ions, we measured the number of ions in trap #2 during the period when the ions were supposed to be separated into trap #2 and trap #4. Our detection optics collected fluorescence photons only from trap #2. After applying Doppler cooling to any ions present in trap #2 for 2 ms we probed them with the detection and repump lasers. This determined the number of ions present in trap #2 independent of their internal state. Figure 4 shows a histogram resulting from a run consisting of 5050 consecutive separation experiments. The horizontal axis is the number of detected photons recorded in an experiment; the vertical axis displays the number of experiments in which that number was detected. The distributions (0, 1, and 2 ion) for different ion numbers are shown for reference. By fitting the data to these distributions we determined that in 95 ± 1 % of the experiments one ion was in trap #2. In 4 ± 1% of the experiments no ions were in trap #2 and in less than 1% of the experiments two ions were in trap #2. We found that we could pick off any number of ions (0, 1, or 2) and move them to trap #2 by changing the bias potential between electrodes 1 and 5. A change of bias on the order of 25 mV adjusted the ion split. The asymmetry observed for the data of Fig. 4 resulted from our inability to precisely control this offset. Finally, with three ions we saw the photon levels corresponding to 0, 1, 2, or 3 ions in trap #2 as we changed the bias between electrodes 1 and 5.

We also measured the energy gained by an ion due to the separating process. Because the ions gained many quanta, the sideband-comparison measurement technique was no longer sensitive. Instead we used stimulated-Raman carrier ($|\downarrow\rangle|n_z\rangle \leftrightarrow |\uparrow\rangle|n_z\rangle$) transitions in the $|n_z\rangle$-state sensitive 90° geometry with $\Delta\vec{k}$ aligned along the trap axis [8, 37]. After separating

[††] For a single ion subjected to the same process, the axial frequency goes to zero at the center of the trap before the double well forms. However for two ions held apart by the Coulomb interaction, neither the center-of-mass nor symmetric-stretch mode frequencies go through zero.

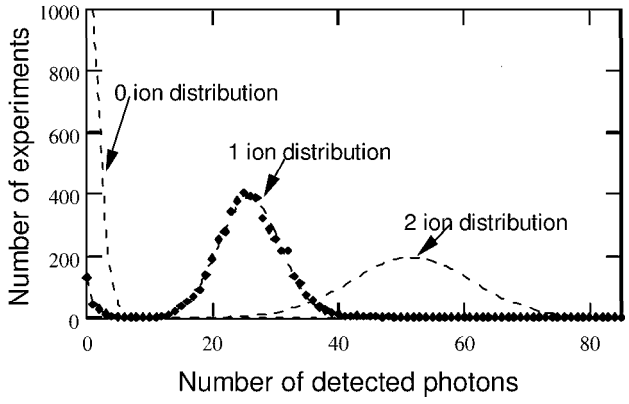

Fig. 4. Histogram of the number of photons detected in a 200 μs time interval for 5050 separation experiments. The distributions of the photon counts for 0, 1, and 2 ions detected are shown as well. The 0-ion distribution extends to 3030 for the 0-photon bin.

the two ions into trap #2 and trap #4 we drove Raman carrier transitions on the ion in trap #2. The final state population of the ion in trap #2 was measured with a standard detection pulse. Figure 5 shows the oscillation in detected photon counts (proportional to the final state population) as a function of the Raman pulse duration. The populations of different $|n_z\rangle$-states oscillate at different rates [8, 37] so the state population for the "hot" separated ion (a state with a distribution of many $|n_z\rangle$-states for an ensemble of experiments) made about half an oscillation before the different $|n_z\rangle$ state oscillation periods averaged to the midway level (half $|\uparrow\rangle$ and half $|\downarrow\rangle$). Also shown in Figure 5 are data from a single ion prepared in $|\downarrow\rangle$ and cooled to near the ground state in trap #2. By comparing the time of the first midway level crossing in the figure for the separated-ion data to that for the "cold" ion data we estimated the average value of n_z for the separated ion. Assuming a thermal distribution of n_z levels we found the average $\langle n_z\rangle$ for the separated ion to be 140 $\pm$ 70 quanta.

The 10 ms separation time minimized the observed heating during separation. At the present time, we do not understand why this time could not be shorter. However, we did observe that most of the energy increase occurred when the center-of-mass frequency was smallest. This was verified by allowing the separation process to evolve only to a certain point, reversing it, and then measuring the ions' temperature. In this way we have an approximate measure of the heating integrated up to the time of reversal. This measurement revealed that the energy increased sharply near the point where the center-of-mass frequency was smallest. This increase in heating at lower frequencies can be expected for two reasons. First, the heating (in terms of quanta per unit of time) increases as ν_z^{-1} even for a uniform noise spectrum. Moreover, Johnson noise from the *RC* filters and any noise injected externally on the control electrodes will increase substantially at lower frequencies due to the reduced efficiency of the filters. This was supported by experiments where we measured the single-ion heating at axial frequencies below 1 MHz, observing that the heating increased more strongly than ν_z^{-3}. Future studies will have to address the causes of heating at lower frequencies and its dependence on ν_z.

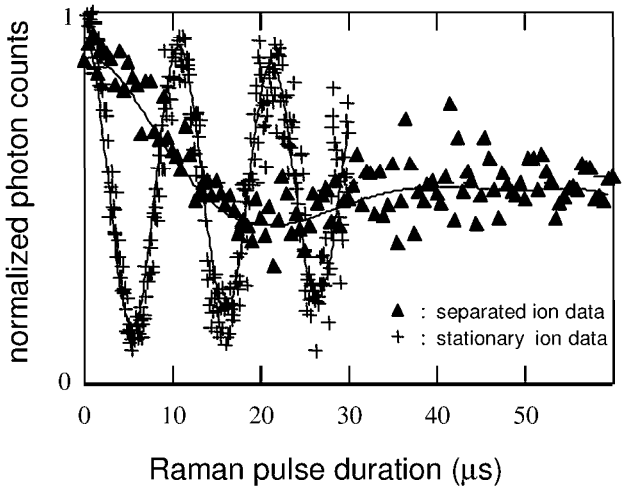

Fig. 5. Photon counts detected as a function of the Raman (carrier) pulse duration. Data for a "hot" separated ion and a single cold ion that has not been moved are shown. The separated-ion data are connected with a smooth curve to guide the eye. The cold ion data are fit with the expected curve to give $\langle n_z \rangle = 0.16$.

8. Summary and Conclusions

In these experiments, we have demonstrated some of the key elements for scaling up an ion-trap quantum processor based on the idea of moving ion qubits between nodes of a multiplexed trap array [8, 26]. We have adiabatically transferred (no motional heating) an ion between two distinct traps, 1.2 mm apart, in approximately 50 μs. We have transferred a single ion between these traps more than 10^6 consecutive times and have observed no loss due to transfer. We measured the fringe contrast in a Ramsey-type experiment where an ion was transferred back and forth between two traps; the measured loss of contrast from transfer was 0.2 ± 0.6 %. Therefore, within experimental error, the internal state coherence of the ion was preserved during transfer. In addition, we demonstrated the separation of two ions, initially held in one trap, into two distinct traps 1.2 mm apart. The separation process took 10 ms and was successful 95% of the time. We measured the energy gained by the ions due to separation to be approximately 150 quanta assuming a thermal distribution of the final motional levels. Finally, we have seen a reduction in the motional heating compared to previous traps [27] by a factor of approximately 100. This improvement appears to be related to the integrity of the trap electrode surfaces and may have been due to preventing deposition of beryllium on the electrodes and/or insuring more complete coating of the electrodes substrates with gold.

The heating that was observed upon separating ions was not unanticipated; to combat it, we expect that some sort of sympathetic cooling must be employed [8]. On the other hand, we believe that it can be reduced and the separation time decreased substantially in future experiments. For example, the geometry of this trap is not well-suited for separating ions. At the minimum center-of-mass axial trap frequency during separating ($\sim$90 kHz) the ions are separated by about 50 μm. Yet, in the experiments reported here, we effectively insert an

approximately 800 μm wide potential wedge between them at this point, making separation very sensitive to small field offsets. If we employ electrode dimensions where the distance from the ion to the nearest electrode is about 50 μm, this should make the width of wedge approximately equal to this distance and make electrode voltage control much less stringent. Of course, in the past [27], motional heating has been observed to increase significantly as the trap dimensions are reduced. However, by taking further steps to insure the integrity of the electrode surfaces, we believe that making smaller traps can lead to efficient separation without significant heating. To minimize heating that might result from smaller dimensions, we note that the separation could be performed in specific locations of the trap array where the dimensions are much smaller than in the accumulator and storage regions.

Optical forces might also be used to facilitate separation (and transfer) as has been demonstrated for neutral atoms [19, 20]. A high-intensity, far-detuned focused laser beam could be applied to the logical qubit ions to exert an optical-dipole force without causing significant dephasing or decoherence due to spontaneous emission. An alternative approach would be to apply optical forces to the cooling ions used for sympathetic cooling. One version of this idea would be to make a logical qubit "packet" where two cooling ions would surround each physical qubit or each logical qubit encoded into a set of physical qubits. Each packet would be kept intact as it is moved through the device by applying optical forces to the cooling ions. This would have the advantage that near-resonant optical-dipole or spontaneous scattering forces could be applied to the cooling ions thereby reducing the laser intensity required for a given force. Although spontaneous emission of the cooling ions would be relatively high, it would not significantly affect the qubit ions, particularly if the qubit and cooling ion transition frequencies are substantially different. When separation with minimal heating is achieved, exciting possibilities such as complex entanglement studies, repetitive error correction, and quantum computing may become practical.

Acknowledgements

This work was supported by the U. S. National Security Agency (NSA) and Advanced Research and Development Activity (ARDA) under Contract No. MOD-7171.00, the U. S. Office of Naval Research (ONR), and the U. S. National Reconnaissance Office (NRO). We thank M. Barrett, D. Lucas, D. Smith, and D. Sullivan for helpful comments on the manuscript.

References

1. S. Lloyd (1993), *A potentially realizable quantum computer*, Science **261**, pp. 1569-1571.
2. J. I. Cirac, P. Zoller, H. J. Kimble, and H. Mabuchi (1997), *Quantum State Transfer and Entanglement Distribution among Distant Nodes in a Quantum Network* Phys. Rev. Lett. **78**, pp. 3221-3224.
3. T. Pellizzari (1997), *Quantum networking with optical fibers*, Phys. Rev. Lett. **79**, pp. 5242-5245.
4. R. G. DeVoe (1998), *Elliptical ion traps and trap arrays for quantum computation*, Phys. Rev. A **58**, pp. 910-914.
5. J. M. Kikkawa and D. D. Awschalom (1999), *Lateral drag of spin coherence in gallium arsenide*, Nature **397**, pp. 139-141.
6. C. Barnes, J. M. Shilton, and A. M. Robinson (2000), *Quantum computation using electrons trapped by surface acoustic waves*, Phys. Rev. B **62**, pp. 8410-8419.

7. P. Recher, E. V. Sukhhorukov, and D. Loss (2001), *Andreev tunneling, Coulomb blockade, and resonant transport of nonlocal spin-entangled electrons*, Phys. Rev. B **63**, pp. 165314-1-11.
8. D. J. Wineland, C. Monroe, W. M. Itano, D. Leibfried, B. E. King, and D. M. Meekhof (1998), *Experimental issues in coherent quantum-state manipulation of trapped atomic ions*, J. Res. Natl. Inst. Stand. Technol. **103**, pp. 259-328.
9. J. I. Cirac and P. Zoller (2000), *A scalable quantum computer with ions in an array of microtraps*, Nature **404**, pp. 579-581.
10. M. J. Renn, D. Montgomery, O. Vdovin, D. Z. Anderson, C. E. Wieman, and E. A. Cornell (1995), *Laser-guided atoms in hollow-core optical fibers*, Phys. Rev. Lett. **75**, pp. 3253-3256.
11. J. Denschlag, D. Cassettari, and J. Schmiedmayer (1999), *Guiding neutral atoms with a wire*, Phys. Rev. Lett. **82**, pp. 2014-2017.
12. D. Müller, D. Z. Anderson, R. J. Grow, P. D. D. Schwindt, and E. A. Cornell (1999), *Guiding neutral atoms around curves with lithographically patterned current-carrying wires*, Phys. Rev. Lett. **83**, pp. 5194-5197.
13. N. H. Dekker, C. S. Lee, V. Lorent, J. H. Thywissen, S. P. Smith, M. Drndi, R. M. Westervelt, and M. Prentiss (2000), *Guiding neutral atoms on a chip*, Phys. Rev. Lett. **84**, pp. 1124-1127.
14. J. Fortagh, H. Ott, A. Grossmann, C. Zimmermann (2000), *Miniaturized magnetic guide for neutral atoms*, Appl. Phys. B **70**, pp. 701-708.
15. M. Key, I. G. Hughes, W. Rooijakkers, B. E. Sauer, and E. A. Hinds (2000), *Propagation of cold atoms along a miniature magnetic guide*, Phys. Rev. Lett. **84**, pp. 1371-1373.
16. D. Cassettari, A. Chenet, R. Folman, A. Haase, B. Hessmo, P. Krüger, T. Maier, S. Schneider, T. Calarco, J. Schmiedmayer (2000), *Micromanipulation of neutral atoms with nanofabricated structures*, Appl. Phys. B **70**, pp. 721-730.
17. Dirk Müller, Eric A. Cornell, Marco Prevedelli, Peter D. D. Schwindt, Ying-Ju Wang, and Dana Z. Anderson (2001), *Magnetic switch for integrated atom optics*, Phys. Rev. A. **63**, 041602(R).
18. J. Reichel, W. Hänsel, and T. W. Hänsch (1999), *Atomic micromanipulation with magnetic surface traps*, Phys. Rev. Lett. **83**, pp. 3398-3401.
19. D. Schrader, S. Kuhr, W. Alt, M. Müller, V. Gomer, D. Meschede (2001), *An optical conveyor belt for single neutral atoms*, Appl. Phys. B **73**, pp. 819 -824.
20. T. L. Gustavson, A. P. Chikkatur, A. E. Leanhardt, A. Görlitz, S. Gupta, D. E. Pritchard, and W. Ketterle (2002), *Transport of Bose-Einstein condensates with optical tweezers*, Phys. Rev. Lett. **88**, 020401.
21. J. D. Prestage, R. L. Tjoelker, G. J. Dick, and L. Maleki (1994), *Improved linear ion trap physics package*, Proc. 1993 IEEE Frequency Control Symposium, pp. 144-147. and J. D. Prestage, R. L. Tjoelker, and L. Maleki (2001), *Recent developments in microwave ion clocks*, Topics Appl. Phys. **79**, pp. 195-211.
22. G. R. Guthöhrlein, M. Keller, K. Hayasaka, W. Lange, and H. Walther (2001), *A single ion as a nanoscopic probe of an optical field*, Nature **414**, pp. 49-51.
23. J. I. Cirac and P. Zoller (1995), *Quantum computations with cold trapped ions*, Phys. Rev. Lett. **74**, pp. 4091-4094.
24. A. Steane, C. F. Roos, D. Stevens, A. Mundt, D. Leibfried, F. Schmidt-Kaler, and R. Blatt (2000), *Speed of ion-trap quantum-information processors* Phys. Rev. A **62**, pp. 042305-1-9.
25. D. G. Enzer, M. M. Schauer, J. J. Gomez, M. S. Gulley, M. H. Holzscheiter, P. G. Kwiat, S. K. Lamoreaux, C. G. Peterson, V. D. Sandberg, D. Tupa, A. G. White, and R. J. Hughes (2000), *Observation of power-law scaling for phase transitions in linear ion crystals*, Phys. Rev. Lett. **85**, pp. 2466-2469.
26. D. Kielpinski, C. Monroe, and D. J. Wineland (2002), *Architecture for a large-scale ion-trap quantum computer*, submitted to *Nature*.
27. Q. A. Turchette, D. Kielpinski, B. E. King, D. Leibfried, D. M. Meekhof, C. J. Myatt, M. A. Rowe, C. A. Sackett, C. S. Wood, W. M. Itano, C. Monroe, and D. J. Wineland (2000), *Heating of trapped ions from the quantum ground state*, Phys. Rev. A **61**, pp. 063418-1-8.
28. D. J. Berkeland, J. D. Miller, J. C. Bergquist, W. M. Itano, and D. J. Wineland (1998), *Mini-*

mization of ion micromotion in a Paul trap, J. Appl. Phys. **83**, pp. 5025-5033.
29. S. R. Jefferts, C. Monroe, E. W. Bell, and D. J. Wineland (1995), *Coaxial-resonator-driven RF (Paul) trap for strong confinement*, Phys. Rev. A **51**, pp. 3112-3116.
30. C. Monroe, D. M. Meekhof, B. E. King, W. M. Itano, and D. J. Wineland (1995), *Demonstration of a fundamental quantum logic gate*, Phys. Rev. Lett. **75**, pp. 4714-4717.
31. B. E. King, C. S. Wood, C. J. Myatt, Q. A. Turchette, D. Leibfried, W. M. Itano, C. Monroe, and D. J. Wineland (1998), *Cooling the collective motion of trapped ions to initialize a quantum register*, Phys. Rev. Lett. **81**, pp. 1525-1528.
32. D. M. Meekhof, C. Monroe, B. E. King, W. M. Itano, and D. J. Wineland (1996), *Generation of nonclassical motional states of a trapped atom*, Phys. Rev. Lett. **76**, pp. 1796-1799.
33. C. A. Sackett (2001), *Quantum information experiments with trapped ions: status and prospects*, Quant. Inf. Comp. **1**, pp. 57-80.
34. M. A. Rowe, D. Kielpinski, V. Meyer, C. A. Sackett, W. M. Itano, C. Monroe, and D. J. Wineland (2001), *Experimental violation of a Bell's inequality with efficient detection*, Nature **409**, pp. 791-794.
35. H. Rohde, S. T. Gulde, C. F. Roos, P. A. Barton, D. Leibfried, J. Eschner, F. Schmidt-Kaler, and R. Blatt (2001), Sympathetic ground-state cooling and coherent manipulation with two-ion crystals, J. Opt. B: Quantum Semiclass. Opt. **3** pp. S34 - S41.
36. Q. A. Turchette, C. J. Myatt, B. E. King, C. A. Sackett, D. Kielpinski, W. M. Itano, C. Monroe, and D. J. Wineland (2000), *Decoherence and decay of motional quantum states of a trapped atom coupled to engineered reservoirs*, Phys. Rev. A **62**, pp. 053807-1-22.
37. H. C. Nägerl, Ch. Roos, D. Leibfried, H. Rohde, G. Thalhammer, J. Eschner, F. Schmidt-Kaler, and R. Blatt (2000), *Investigating a qubit candidate: Spectroscopy on the $S_{1/2}$ to $D_{5/2}$ transition of a trapped calcium ion in a linear Paul trap*, Phys. Rev. A **61**, 023405-1-9.